

Neural Simpletrons – Minimalistic Probabilistic Networks for Learning With Few Labels

Dennis Forster^{1*}, Abdul-Saboor Sheikh^{2,3*}, Jörg Lücke³

forster@fias.uni-frankfurt.de, sheikh.abdulsaboor@gmail.com, joerg.luecke@uni-oldenburg.de

¹ Frankfurt Institute for Advanced Studies (FIAS), Frankfurt am Main, Germany

² Technical University of Berlin, Berlin, Germany

³ Carl von Ossietzky University of Oldenburg, Oldenburg, Germany

*joined first authorship

Abstract

Deep learning is intensively studied from both the perspectives of unsupervised and supervised learning approaches. The combination of the two learning schemes is typically done using separate algorithms, often resulting in complex and heterogeneous systems that are equipped with large numbers of tunable parameters. In this work we study the potential of a tighter integration of unsupervised and supervised learning, and empirically highlight the model complexity vs. performance tradeoff. We aim at defining the most minimalistic system that learns from labeled and unlabeled data. First we derive neural update and learning rules based on an hierarchical Poisson mixture model for classification. The network is then scaled using standard deep learning techniques. We use the task of learning from data with few labels as a natural task in between unsupervised and supervised approaches. In quantitative evaluations on standard benchmarks, we find that a tighter integration of unsupervised and supervised learning results in very competitive performance for the minimalistic approach studied here. Furthermore, the used monolithic learning is amongst the least complex of all competitive approaches (lowest numbers of tunable parameters). Finally, in the limit of very few labels, we demonstrate applicability where other competitive systems have not been reported to operate, so far. In general, our study argues in favor of a stronger focus and integration of unsupervised learning in order to simplify and improve the capabilities of current deep learning approaches.

1 Introduction

The field of deep neural networks has rapidly evolved over the last decade, with significant progress on both the modeling and the application side. Important standard models are Deep Belief Networks (DBN; [1]), convolutional neural networks (CNN; [2, 3]), Deep Boltzmann Machines (DBM, [4]) or deep autoencoders (e.g.[5]). The often hybrid use of unsupervised and supervised learning routines, e.g., in DBNs or DBMs and many other systems often make comparisons of the systems themselves difficult. A strong focus on benchmark results presumably originates from these difficulties, with the MNIST dataset being the most prominent example. Comparison is further complicated by often large sets of tunable parameters. These range from: (i) parameters for the network architecture itself (number of layers, units per layer); (ii) parameters for data preprocessing; (iii) parameters for weight initialization; (iv) parameters defining the non-linearities between layers; (v) parameters for number of samples, initialization and burn-in times (for sampling based systems); (vi) parameters for enforced

sparsity (of activity and/or connectivity); (vii) parameters for annealing schedules; (viii) parameters to prevent overfitting (regularization parameters, parameters of drop-out, early stopping); (ix) parameters for integrated dimensionality reduction algorithms and so on. The tuning of free parameters can therefore be considered as an additional optimization procedure (compare [6, 7]) usually requiring additional information, e.g., in the form of extra labels. Some of the above listed parameters can and have been treated in theoretically grounded ways. For instance, network architectures can be treated using hyperpriors which allows to translate the corresponding free parameters to hyper-parameters (e.g. [8]). Also many regularization parameters find their correspondences in prior parameters of probabilistic generative models, and can as such be learned from data (e.g., [9, 10, 11] and others). Maybe most importantly, however, hierarchical generative models provide a grounded way to learn from unlabeled data as they seek to optimize the data likelihood. Probabilistic directed graphical models of feature hierarchies therefore offer themselves as high-potential alternatives to discriminative deep learning, with principled ways to learn all model parameters.

Here we aim at a minimalistic approach to combine unsupervised and supervised learning in deep networks: we derive a neural network model from an elementary hierarchical mixture model. The network thereby inherits full probabilistic interpretability, a minimal number of tunable parameters, and it is scalable to large data and network sizes. As such it allows for an investigation of (A) the interplay of unsupervised and supervised learning, and (B) for a comparison with standard and most recent deep networks on task with few labels.

2 A normalized hierarchical mixture model

A classification problem can be canonically modeled as inference based on a probabilistic mixture model. Such a model should be hierarchical or *deep* if we expect the data to have a hierarchical structure. For hand-written digits, for instance, we first expect the data to be structured by the process of deciding for a digit class ('0' to '9'), and second we expect structure within each class according to different writing styles.

A minimalistic generative model. While further structure can be expected for most data, a minimalistic deep model is a directed graphical model with two hidden and one observed layer:

$$p(k|\pi) = \frac{1}{K}, \quad p(l|k) = \delta_{lk} \quad (1)$$

$$p(c|k, \mathcal{R}) = \mathcal{R}_{kc}, \quad \sum_c \mathcal{R}_{kc} = 1 \quad (2)$$

$$p(\vec{y} | c, \mathcal{W}) = \prod_d \text{Poisson}(y_d; \mathcal{W}_{cd}), \quad \sum_d \mathcal{W}_{cd} = A \quad (3)$$

The top layer of the model allows for representation of K abstract concepts or super classes (e.g., digits '0' to '9') comprising the data, while a middle layer is introduced to encapsulate any of the occurring C subclasses (e.g., different writing styles of the digits). The final layer represents an observed data sample generated by the model according to a Poisson distribution, i.e., in line with typical Deep Learning models we assume positive observed data. Note that while the normalization of the rows of \mathcal{R} is required for normalized categorical distributions, the normalization of the rows of \mathcal{W} represents an additional constraint. By constraining the weights to sum to a constant A , the model expects contrast normalized data. If the dimensionality D of the observed data is sufficiently large, we can simply normalize the data such that $\sum_d y_d = A$ in order to fulfill the constraint.

Maximum likelihood learning. Given N data points $\vec{y}^{(n)} \in \mathbb{R}_+^D$ and $\sum_d y_d^{(n)} = A$, we seek parameters $\Theta = (\mathcal{W}, \mathcal{R})$ of the model eqs. (1) to (3) that maximize the data (log-)likelihood

$$\mathcal{L}(\Theta) = \sum_{n=1}^N \log \left(\sum_{c=1}^C \left(\left(\prod_{d=1}^D \frac{\mathcal{W}_{cd}^{y_d^{(n)}} e^{-\mathcal{W}_{cd}}}{\Gamma(y_d^{(n)}+1)} \right) \sum_{k \in l^{(n)}} \frac{\mathcal{R}_{kc}}{K} \right) \right). \quad (4)$$

We further assume that some of the data may also come labeled. This implies that whenever the label $l^{(n)}$ is known for a data point $\vec{y}^{(n)}$, the summation over k in (4) gets marginalized to R_{lc} .

To find likelihood maximizing values of Θ , we can apply the Expectation Maximization (EM) algorithm. EM iteratively increases the free energy, which can be shown to be a tight lower bound of the log-likelihood in our case (see appendix B for details). Parameter update equations (the M-step) can canonically be derived by setting free energy derivatives to zero. Our parameter updates are given by:

$$\mathcal{W}_{cd} = A \frac{\sum_n p(c|\vec{y}^{(n)}, l^{(n)}, \Theta^{\text{old}}) y_d^{(n)}}{\sum_{d'} \sum_n p(c|\vec{y}^{(n)}, l^{(n)}, \Theta^{\text{old}}) y_{d'}^{(n)}}, \quad \mathcal{R}_{kc} = \frac{\sum_n p(k|l^{(n)}) p(c|\vec{y}^{(n)}, l^{(n)}, \Theta^{\text{old}})}{\sum_{c'} \sum_n p(k|l^{(n)}) p(c'|\vec{y}^{(n)}, l^{(n)}, \Theta^{\text{old}})}, \quad (5)$$

where only labeled data is taken into account for updates of \mathcal{R}_{kc} .

3 A neural network for optimal hierarchical learning

Without diverging from the aforementioned maximum likelihood solution, if we want to transform learning such that it can happen in real-time, e.g., for large-scale or online scenarios, we have to find a valid online regime to replace the batch mode update eqs. (5). A further motivation for deriving online learning is its coherence with learning in neural circuits; given proper learning rules and interaction between different layers and units of the model, the derived online learning method can be shown to take a neurally plausible form. To formulate such an online algorithm we make use of earlier results in [12] and [13], who derived neural online learning equations that converge to the batch-mode EM-based learning in a dual-layer mixture model. Here we extend the previous findings to derive a neural network analog to the hierarchical generative model shown in sec. 2.

A neural network approximation. Consider the neural network in fig. 1 with neural activities \vec{y} , \vec{s} and \vec{t} . We assume the data points \vec{y} to be obtained from a set of unnormalized data points $\tilde{\vec{y}}$, and the label information to be presented as top-down input vector \vec{u} as follows:

$$y_d = (A - D) \frac{\tilde{y}_d}{\sum_{d'} \tilde{y}_{d'}} + 1 \quad u_k = \begin{cases} p(k|l) = \delta_{kl} & \text{for labeled data} \\ p(k) = \frac{1}{K} & \text{for unlabeled data} \end{cases} \quad (6)$$

Furthermore, we assume the neural activities \vec{s} and \vec{t} to be normalized as well (i.e., $\sum_d y_d = A$, $\sum_k u_k = 1$, $\sum_d s_c = B$, and $\sum_k t_k = B'$). For all weights of the network we assume Hebbian learning with a subtractive synaptic scaling term:

$$\Delta W_{cd} = \epsilon_w (s_c y_d - s_c W_{cd}) \quad \Delta R_{kc} = \epsilon_r (t_k s_c - t_k R_{kc}). \quad (7)$$

By taking sums over c and over k respectively, we find that $\sum_d W_{cd}$ converges to A and $\sum_c R_{kc}$ converges to B . If we now, because of this result, assume the weights W and R to be normalized to A and B respectively, we can show that an iterative application of online learning in eqs. (7) finally results in the weights W and R to satisfy the following equations at convergence:

$$W_{cd} \approx A \frac{\sum_n s_c^{(n)} y_d^{(n)}}{\sum_{d'} \sum_n s_c^{(n)} y_{d'}^{(n)}} \quad R_{kc} \approx B \frac{\sum_n t_k^{(n)} s_c^{(n)}}{\sum_{c'} \sum_n t_k^{(n)} s_{c'}^{(n)}}, \quad (8)$$

where $\vec{y}^{(n)}$ is the n th datapoint, and $\vec{s}^{(n)}$ and $\vec{t}^{(n)}$ are the hidden neural activities given $\vec{y}^{(n)}$ and $\vec{u}^{(n)}$. Eqs. (8) become exact in the limit of small learning rates $\epsilon_{W/R}$ in eqs. (7) and large numbers of data points N . The derivations are done through a series of approximations including Taylor expansion and the geometric series. Technical details are given in appendix C.

For the normalization assumptions demanded above, eqs. (8) apply for any neural activation rules for s_c and t_k as long as learning converges. For our purposes, we identify s_c with the posterior probability

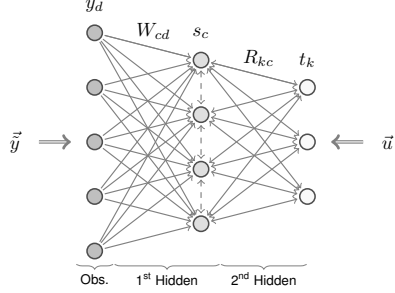


Figure 1: Graphical illustration of the hierarchical recurrent neural network model.

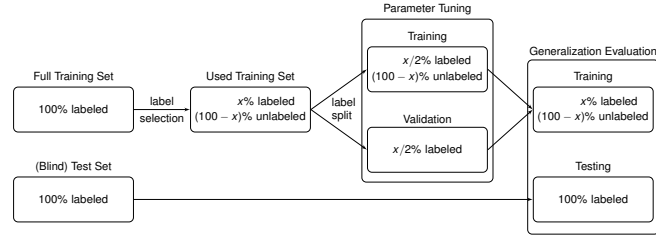


Figure 2: Parameter tuning, training and testing protocol for the NeSi algorithms.

$p(c|\vec{y}, l, \Theta)$ and t_k with the posterior probability $p(k|l)$ in eqs. (5). A comparison of eqs. (8) with M-step eqs. (5) shows that such neural online learning is equal to EM-learning at convergence (note that $B = B' = 1$ as s_c and t_k sum to one).

The computation of posteriors is in general a difficult and computationally intensive part, and their interpretation as neural activation rules may be difficult. Because of a specific interplay between introduced constraints, categorial distribution and Poisson noise, the posteriors that have to be computed in our case greatly simplify.

The posterior $p(c|\vec{y}, l, \Theta)$ identified with the neural activities s_c reduces to:

$$s_c = \frac{\exp(I_c)}{\sum_{c'} \exp(I_{c'})} \quad \text{with } I_c = \sum_d \log(\mathcal{W}_{cd}) y_d + \log\left(\sum_k u_k \mathcal{R}_{kc}\right). \quad (9)$$

Considering eq. (9), we can interpret I_c as input to neural unit s_c . The input consists of a bottom-up and a top-down activation. The bottom-up input is the standard weighted summation of neural networks (note that we could redefine the weights by $\tilde{\mathcal{W}}_{cd} := \log(\mathcal{W}_{cd})$). Likewise, the top-down input is a standard weighted sum, $\sum_k u_k \mathcal{R}_{kc}$, but affects the input through a logarithm. Both sums can be computed locally at the neural unit c . The inputs to the hidden units s_c are then combined using a softmax function, which is also standard for neural networks. Here, the softmax is not imposed ad-hoc, however, but is a direct result from the generative mixture model.

The other posterior $p(k|l)$ identified with t_k assumes labeled data (i.e., like in the M-step of the generative model, we will update the weights \mathcal{R}_{kc} only for labeled data). For unlabeled data, we can identify the activities t_k with the posterior $p(k|\vec{y}, \theta)$:

$$t_k = \delta_{kl} \quad \text{for labeled data,} \quad t_k = \sum_c \frac{\mathcal{R}_{kc}}{\sum_{k'} \mathcal{R}_{k'c}} s_c \quad \text{for inference.} \quad (10)$$

The set of all eqs. (6), (7), (9) and (10) thus represent the definition of a neural network with bottom-up/top-down integration in the middle layer and local neural learning rules. Because of our above derivations, the neural activities \vec{s} and \vec{t} are directly interpretable as posterior probabilities w.r.t. the hierarchical mixture model of sec. 2. Crucially, online learning in eqs. (7) has the same convergence points as EM learning for the mixture model. However, in finite distances from the convergence points, neural learning follows different gradients, i.e., the trajectories of the network in parameter space are different from EM. By using different learning rates in eqs. (7), the gradient directions can even be changed in a systematic way without changing the convergence points.

Note that the equations defining the neural network are elementary, very compact, and they contain a minimal number of four free parameters: ϵ_W , ϵ_R (learning rates), input normalization constant A , and number of hidden units C . All numerical experiments will be based on eqs. (6), (7), (9) and (10), and because of its compactness we will refer to the network as *Neural Simpletron*.

4 Numerical experiments

We apply an efficiently scalable implementation of our network¹ to two widely used benchmarks for classification, the 20 Newsgroups text dataset and the dataset of handwritten digits MNIST. For investigating the task of learning from weakly labeled data, we randomly divide the training parts of the datasets into labeled and unlabeled partitions. We make sure that each class has the same number of examples in the labeled part of the training set. We repeat experiments for different proportions of labeled data and measure the classification error on the test set. For each label proportion setting, we report an average classification error computed over 10 independent runs with random labeled and unlabeled data splits. We will refer to our method eqs. (6), (7), (9) and (10) as r-NeSi. To investigate the effect of top-down recurrent information in our network, we will also test a feed-forward version of the network, where we will simply prune the top-down weights in eq. (9) (i.e., I_c will only contain the feed-forward term). This version will be referred to as ff-NeSi. Since ff-NeSi is stripped of the top-down recurrency, the network can be trained disjointly using a greedy layer-by-layer approach, which is customary for deep networks.

Learning from weakly labeled data. The second hidden layer of the NeSi algorithms is trained fully supervised, i.e., it is only updated by data points $\vec{y}^{(n)}$ for which a label $l^{(n)}$ is available. However the first hidden layer, with a much higher dimensionality (a factor D/K of 3059.4 for 20 Newsgroups and 78.4 for MNIST), is trained on both labeled and unlabeled data. While in the feed-forward network the first hidden layer is trained disjointly fully unsupervised, in the recurrent formulation the network is able to incorporate additional class information flowing-in from the top layer to derive learning into a more discriminative regime.

Parameter tuning. Availability of only few labels has to be taken into account on both training of the model as well as tuning of free parameters. In our experiments we take a subset of the training data for the tuning of our free parameters, which are: learning rates $\epsilon_{W/R}$, the normalization constant A and the number of hidden units C . To construct the dataset for parameter tuning we randomly pick 10 labeled data points per class (i.e., 200 for 20 Newsgroups and 100 labeled data for MNIST). We keep half of the labeled data for validation and use the other labeled half (plus all unlabeled training data) as training set for parameter tuning. Once tuned, the free parameters then remain fixed for all the reported experiments. This way we ensure, that our results are actually achieved by using no more than the labels provided within the training set and with no additional knowledge about performance on the test set. The general tuning, training and testing protocol is shown in fig. 2.

Initialization details. For the complete setting, where there is a good amount of labeled data per hidden unit even in the weakly labeled setting, and the risk of running into early local optima where the classes are not well separated is high, we initialize the weights of the first hidden layer in a modified version of [13] by computing the mean m_{kd} and standard deviation σ_{kd} of the labeled training data for each class k and setting $W_{kd} = m_{kd} + \mathcal{U}(0, 2\sigma_{kd})$ where $\mathcal{U}(x_{dn}, x_{up})$ denotes the uniform distribution in the range (x_{dn}, x_{up}) .

For the highly overcomplete setting, where there are far less labeled data points than hidden units in the weakly labeled setting, and class separation is no imminent problem, we initialize the weights using all data disregarding the label information. With the mean m_d and standard deviation σ_d over all training data points we set $W_{cd} = m_d + \mathcal{U}(0, 2\sigma_d)$.

The weights of the second hidden layer are always initialized as $R_{kc} = 1/C$.

Document classification (20 Newsgroups). The 20 Newsgroups dataset in the ‘bydate’ version consists of 18 774 newsgroup documents belonging to 20 different classes of newsgroup topics, of which 11 269 form the training set and the remaining 7505 form the test set. Each data vector comprises the raw occurring frequencies of 61 188 words in each document. We preprocess the data using tf-idf weighting.

¹We use a python 2.7 implementation of eqs. (6), (7), (9) and (10) which are optimized using Theano to execute on a NVIDIA GeForce GTX TITAN Black GPU. The source code and scripts for repeating the experiments discussed here are available via <https://github.com/dennisforster/NeSi>.

Table 1: Test error on 20 Newsgroups for different weakly labeled settings using the greedy feed-forward and the recurrent Neural Simpletron

#Labels	ff-NeSi	r-NeSi	HDRBM
200	30.07 ± 0.61	29.19 ± 0.44	
800	27.64 ± 0.13	27.80 ± 0.24	31.8
2000	27.40 ± 0.23	27.98 ± 0.20	
7505	27.53 ± 0.21	27.99 ± 0.34	23.8

No stemming, removals of stop words or frequency cutoffs were applied. We investigate settings of 200, 800 and 2000 labels in total – that is 10, 40 and 100 labels per class, as well as the fully labeled setting. For each setting we present the mean test error, averaged over 10 independent runs.

Results on 20 Newsgroups. Following the tuning, training and testing protocol described in sec. 4, we find optimal values for the free parameters as $C = 20$, $A = 80000$, $\epsilon_w = 5.0 \times C/N$ and $\epsilon_r = 0.5 \times K/L$, where N denotes the total number of training data points and L denotes the number of labels. We used this parameter setting with the initialization procedure described in sec. 4 for all results of the NeSi algorithms shown in tab. 1.

We train our model on a 20-class problem without any feature selection. To the best of our knowledge, most methods that report performance on the same benchmark do consider other tasks: They either break the task into binary classification between individual or merged topics, e.g., [14, 15, 16, 17], and/or perform feature selection, e.g., [18, 19], for classification. There are however works that are compatible with our experimental setup [20, 21]. A hybrid of generative and discriminative RBMs (HDRBM) are trained by [20] using stochastic gradient decent to perform semi-supervised learning. They report results on 20 Newsgroups for both fully and weakly labeled setups. All their model and hyper-parameters are optimized using a validation set of 1691 examples in the fully labeled setting, but for semi-supervised setup 200 examples were used for validation. The classification accuracy of the method is compared in tab. 1.

We also performed experiments with the same parameter setting, but using only one label per class for training. There, the r-NeSi algorithm achieves a test error of $(67.24 \pm 1.97)\%$ and ff-NeSi of $(70.91 \pm 2.20)\%$. For two labels per class, the test error decreases to $(54.52 \pm 2.10)\%$ for r-NeSi and $(53.55 \pm 1.92)\%$ for ff-NeSi.

In the fully labeled setting, changing the initialization procedure to $R_{kc} = \delta_{kc}$ helped to avoid early local optima and the r-NeSi reaches a test error of $(18.40 \pm 0.02)\%$. For this last result however, we had to use a validation set as a subset of the fully labeled training set. This shows, that fine tuning the parameters based on each individual label setting (i.e., using the additional label information not only during training, but also during parameter tuning) and including the initialization procedure as additional free parameter could potentially lead to better parameter settings and stronger performance.

Handwritten digit recognition (MNIST). The MNIST dataset consists of 60 000 training and 10 000 testing data points of 28×28 images of gray-scale handwritten digits which are centered by pixel mass. We perform experiments using 100, 600, 1000 and 3000 labels in total as well as the fully labeled training set. Again, following sec. 4, we find optima for the free parameters at $C = 10\,000$, $A = 900$, $\epsilon_w = 0.2 \times C/N$ and $\epsilon_r = 0.2 \times K/L$.

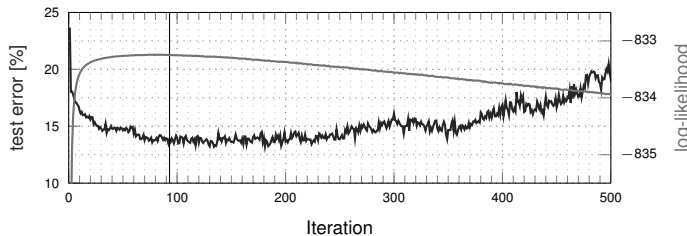


Figure 3: Evolution of test error and log-likelihood during training. Both show a strong negative correlation. The vertical line denotes the stopping point.

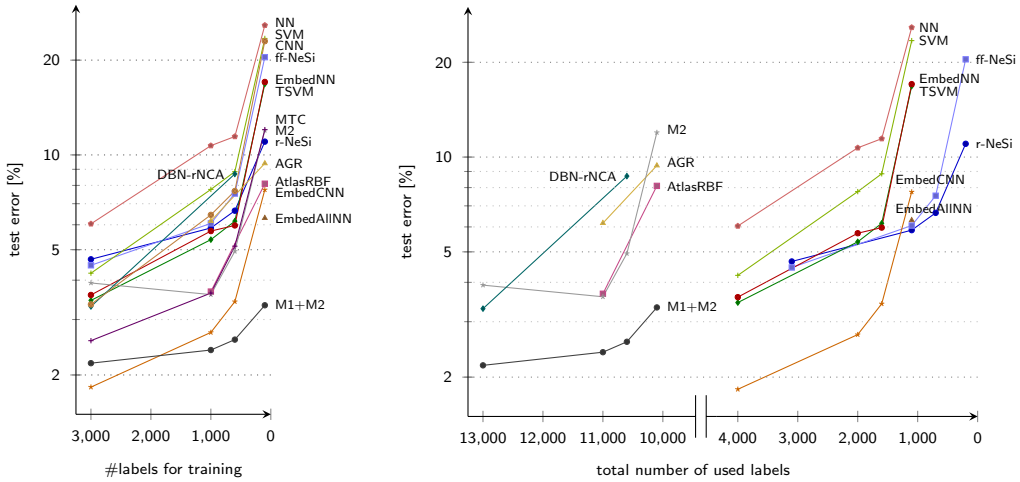


Figure 4: Classification performance of different algorithms compared against varying proportion of weakly labeled training data. The left plot shows the amount of labeled data seen by the compared algorithms during training. The right plot illustrates for the same experiments the amount of labeled data seen by each of the algorithms when their parameter tuning procedures are also taken into account in conjunction with the training.

A stopping criterion against overfitting. Training of the first layer in the feed-forward network is not influenced by the state of the second layer, and is therefore oblivious to the number of provided labels. This is no longer the case for the recurrent network. A low number of labels will in the recurrent network lead to overfitting effects when the number of hidden units in the first layer is substantially larger than the number of labeled data points. Since learning in our network corresponds to maximum likelihood learning in a hierarchical generative model, a natural criterion for early stopping is given by monitoring the data log-likelihood given by eq. (4). As soon as the labeled data starts overfitting the first layer units as a result of top-down influence in I_c , the log-likelihood computed over the whole training data will start to go down. This declining event in data likelihood can be used as stopping criterion to avoid overfitting. Fig. 3 shows the evolution of the log-likelihood per used data point during training compared to the test error. For experiments over a variety of network sizes, we found strong negative correlations on average $\langle \text{PPMCC} \rangle = -0.85 \pm 0.1$. To disregard random fluctuations in the likelihood, we compute the centered moving average over 20 iterations and stop as soon as this value drops below its maximum value by more than the centered moving standard deviation. Here in fig. 3 the test error is only computed for illustration purposes. In our experiments we used the moving average of the likelihood to detect the drop event and stop learning. In our control experiments on MNIST we found out that the best test error generally occurred some iterations after the peak in the likelihood (see fig. 3), which we however disregarded in the reported results.

Results on MNIST. Fig. 5 shows the results of the NeSi algorithms on the MNIST benchmark. As observed the recurrent version (r-NeSi) results in significantly lower classification errors than the feed-forward network (ff-NeSi) in settings with very few labels. In comparison with other standard and recent state-of-the-art approaches our minimalistic approaches are competitive – outperforming recent DBN versions and other approaches. In the light of reduced model complexity and effectively used labels, we can furthermore compare to the few algorithms with a lower error rate.

We made a detailed analysis of all algorithms of fig. 5 to analyze complexity, number of free parameters, training, testing and tuning protocols. Comparison details can be found in appendix D. In summary, most algorithms we compared to in fig. 5 have either seen the test set before classification or use an extra validation set, which exceeds the number of labels available during training. AGR and AtlasRBF may even have used labeled data points of the test set. Seeing the unlabeled test data before classification can be defended by arguing that training on unlabeled test set data is part of the decision procedure. Essentially,

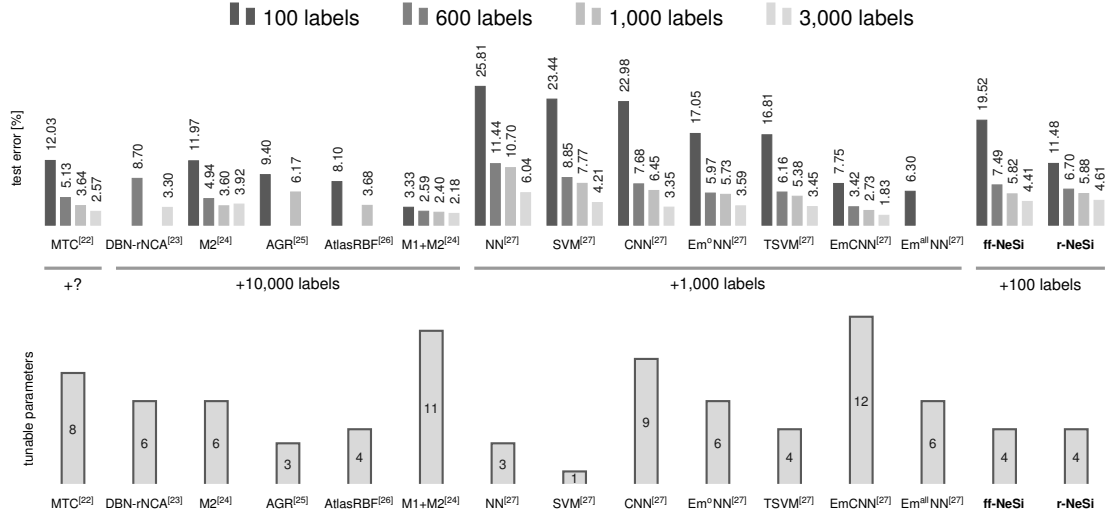


Figure 5: Comparison of different algorithms on weakly labeled MNIST data. The figure shows data if the systems are trained using 100, 600, 1000, and 3000 labeled MNIST data points. The algorithms are of different complexity with different sets of tunable/free parameters (we give estimates here). Algorithms also use different training, testing and tuning protocols (appendix D gives more details).

the decision boundaries for classification are fine-tuned using also test data before classification. A major problem arises, however, if such a “semi-blind” approach is compared to a fully blind approach. Deep learning approaches, for instance, do usually not adjust the trainable parameters on the (unlabeled) test data before classification. All semi-blind approaches discussed above do therefore have an advantage, i.e., the comparison is not fair if additional information about the test set is available only for some methods.

Using a validation set can avoid both seeing any test data and having to tune free parameters on the test set. But if this validation set exceeds the training set, then more information is given to an algorithm than what is available during training. In fig. 5 we grouped the models by the number of additional labeled data points used for parameter tuning and fig. 4 shows the performance of the models with respect to the number of labels used for training and used in total.

For the NeSi approaches we deliberately avoided (A) any training on test set data, (B) any tuning of free parameters on the test set, and (C) a validation set, that exceeds the training set. Since we performed repeated independent training runs to gain meaningful statistical results, and also used different label settings with the same parameter setting, we also consider our validation set as additional labels, as they are not necessarily a subset of the randomly drawn labels for model training. However, by using a validation set with as few labels as available during training, we can assure to be able to find parameter settings for the presented performance using no more labels as given in the respective training settings. Furthermore, this training and tuning schedules assures to not result in an overfitting on the test set. The more free parameters a system uses, the higher the danger of such an overfitting.

We also trained the networks with the same parameter setting but only one label per class. In this setting, the r-NeSi network reaches a test error of $(26.26 \pm 1.59)\%$ and the ff-NeSi of $(54.24 \pm 1.43)\%$. In the fully labeled setting, the r-NeSi algorithm achieves a test error of $(2.93 \pm 0.01)\%$ and the ff-NeSi of $(3.28 \pm 0.02)\%$.

5 Discussion

We have studied a minimalist and monolithic system that learns from unlabeled and labeled data. This served two closely related goals: (1) the study of a tight coupling of unsupervised and supervised learning

at scales of current deep learning models, and (2) the empirical study of model complexity vs. performance tradeoff.

The studied neural network optimizes the likelihood of a directed graphical model with two hidden layers. On the standard MNIST benchmark with few labeled data points, we observed that a minimalistic network derived based on a hierarchical Poisson mixture produces competitive results. Notably, for weakly labeled MNIST it outperforms all standard deep learning approaches (e.g., [1, 2, 3, 4]) as well as SVM approaches (e.g., [28]). Likewise, the network shows better results than HD-RBM [20] for weakly labeled data on 20 Newsgroups (which is not as frequently used). Moreover, the studied networks represent the best performing monolithic systems for classification on weakly labeled data (e.g., on MNIST). In contrast, the standard Deep Learning approaches [1, 2, 3, 4] and their currently best performing variants [23, 24, 27] use hybrid architectures and training protocols, usually involving separate unsupervised and supervised phases; other approaches combine separate algorithms such as manifold learning and classifier optimization (e.g., [26, 27, 29]).

At the same time, our minimalistic approach highlights the tradeoff between model complexity and performance on weakly labeled data. All studied systems, including our own, come with some tunable parameters that have to be set usually by using an additional validation set. Hybrid systems come with larger sets of tunable parameters, and in turn require larger validation sets. As a consequence, the net amount of required labels for such systems increases. Our numerical results argue in favor of taking all required labels (training and validation set labels) into account for model comparison. The net amount can then be taken as a measure for model complexity, and performance measured relative to the net amount naturally penalizes model complexity in a kind of empirical Occam's razor (while any theoretical approaches are difficult for standard deep learning architectures). If the total number of labels is considered, the minimalistic models studied here can be operated down to numbers of labels where none of the other systems has been reported to operate. Considering the results in sec. 4 it has to be emphasized however, that the other compared systems may also perform well for further reduced total numbers. For complex systems though, the larger number of tunable parameters will very likely result in higher numbers of required labels. For the fully labeled case, on the other hand, our minimalistic approach is outperformed by the competing systems, especially by those using back-propagation.

Finally, the competitiveness of the Simpletron networks can be explained by them learning from labeled and unlabeled data using monolithic learning equations. Also in general, directed graphical models provide grounded ways to model data and to integrate unsupervised and supervised learning. Applications have been hindered however, by the challenges involved in scaling inference and learning. The competitive performance observed here can be regarded as evidence for the potential of a tight integration of unsupervised and supervised learning using directed graphical models. We therefore see the presented results as an argument in favor of grounded approaches to integrate unsupervised and supervised learning, and in favor of further research based on directed graphical models.

References

- [1] GE Hinton, S Osindero, and YW Teh. A fast learning algorithm for deep belief nets. *Neural Computation*, 18:1527–1554, 2006.
- [2] Y. LeCun and Y. Bengio. Convolutional networks for images, speech, and time-series. In M. A. Arbib, editor, *The Handbook of Brain Theory and Neural Networks*. MIT Press, 1995.
- [3] Y. LeCun, K. Kavukcuoglu, and C. Farabet. Convolutional networks and applications in vision. *Proc. Symposium on Circuits and Systems*, pages 253–6, 2010.
- [4] Ruslan Salakhutdinov and Geoffrey E Hinton. Deep boltzmann machines. In *International Conference on Artificial Intelligence and Statistics*, pages 448–455, 2009.
- [5] P. Vincent, H. Larochelle, I. Lajoie, Y. Bengio, and P.-A. Manzagol. Stacked denoising autoencoders: Learning useful representations in a deep network with a local denoising criterion. *The Journal of Machine Learning Research*, 11:3371–3408, 2010.
- [6] J. Bergstra, R. Bardenet, Y. Bengio, and B. Kégl. Algorithms for Hyper-Parameter Optimization. 2011.

- [7] C. Thornton, F. Hutter, H. H. Hoos, and K. Leyton-Brown. Auto-WEKA: Combined selection and hyperparameter optimization of classification algorithms. 2013.
- [8] Ryan Prescott Adams, Hanna M Wallach, and Zoubin Ghahramani. Learning the structure of deep sparse graphical models. *arXiv preprint arXiv:1001.0160*, 2009.
- [9] P Berkes, R Turner, and M Sahani. On sparsity and overcompleteness in image models. *Advances in Neural Information Processing Systems*, 21, 2008.
- [10] S. Mohamed, K. Heller, and Z. Ghahramani. Evaluating Bayesian and L1 approaches for sparse unsupervised learning. In *ICML*, 2012.
- [11] Abdul-Saboor Sheikh, Jacquelyn A. Shelton, and Jörg Lücke. A truncated em approach for spike-and-slab sparse coding. *Journal of Machine Learning Research*, 15:2653–2687, 2014.
- [12] J. Lücke and M. Sahani. Maximal causes for non-linear component extraction. *Journal of Machine Learning Research*, 9:1227–67, 2008.
- [13] Christian Keck, Cristina Savin, and Jörg Lücke. Feedforward inhibition and synaptic scaling – two sides of the same coin? *PLoS Computational Biology*, 8:e1002432, 2012.
- [14] David Cheng, Ravi Kannan, Santosh Vempala, and Grant Wang. A divide-and-merge methodology for clustering. *ACM Transactions on Database Systems (TODS)*, 31(4):1499–1525, 2006.
- [15] Do-kyum Kim, Matthew Der, and Lawrence K Saul. A gaussian latent variable model for large margin classification of labeled and unlabeled data. In *AISTATS*, pages 484–492, 2014.
- [16] S. Wang and C. D. Manning. Baselines and bigrams: Simple, good sentiment and topic classification. In *Annual Meeting of the Association for Computational Linguistics: Short Papers-Volume 2*, pages 90–94, 2012.
- [17] Xiaojin Zhu, Zoubin Ghahramani, John Lafferty, et al. Semi-supervised learning using gaussian fields and harmonic functions. In *ICML*, volume 3, pages 912–919, 2003.
- [18] Nitish Srivastava, Ruslan R Salakhutdinov, and Geoffrey E Hinton. Modeling documents with deep boltzmann machines. In *Uncertainty in Artificial Intelligence*, 2013.
- [19] Burr Settles. Closing the loop: Fast, interactive semi-supervised annotation with queries on features and instances. In *Proceedings of the Conference on Empirical Methods in Natural Language Processing*, pages 1467–1478. Association for Computational Linguistics, 2011.
- [20] Hugo Larochelle and Yoshua Bengio. Classification using discriminative restricted boltzmann machines. In *ICML*, pages 536–543, 2008.
- [21] Marc’Aurelio Ranzato and Martin Szummer. Semi-supervised learning of compact document representations with deep networks. In *ICML*, pages 792–799, 2008.
- [22] Salah Rifai, Yann N Dauphin, Pascal Vincent, Yoshua Bengio, and Xavier Muller. The manifold tangent classifier. In *NIPS*, pages 2294–2302, 2011.
- [23] R. Salakhutdinov and G. E. Hinton. Learning a nonlinear embedding by preserving class neighbourhood structure. In *AISTATS*, pages 412–419, 2007.
- [24] D. P. Kingma, S. Mohamed, D. J. Rezende, and M. Welling. Semi-supervised learning with deep generative models. In *NIPS*, pages 3581–3589, 2014.
- [25] Wei Liu, Junfeng He, and Shih-Fu Chang. Large graph construction for scalable semi-supervised learning. In *ICML*, pages 679–686, 2010.
- [26] Nikolaos Pitelis, Chris Russell, and Lourdes Agapito. Semi-supervised learning using an unsupervised atlas. In *Machine Learning and Knowledge Discovery in Databases*, pages 565–580. Springer, 2014.
- [27] J. Weston, F. Ratle, H. Mobahi, and R. Collobert. Deep learning via semi-supervised embedding. In *Neural Networks: Tricks of the Trade*, pages 639–655. Springer, 2012.
- [28] Ronan Collobert, Fabian Sinz, Jason Weston, and Léon Bottou. Large scale transductive svms. *The Journal of Machine Learning Research*, 7:1687–1712, 2006.
- [29] Nikolaos Pitelis, Chris Russell, and Lourdes Agapito. Learning a manifold as an atlas. In *CVPR*, pages 1642–1649. IEEE, 2013.
- [30] Radford Neal and G. Hinton. A view of the EM algorithm that justifies incremental, sparse, and other variants. In M. I. Jordan, editor, *Learning in Graphical Models*. Kluwer, 1998.
- [31] Olivier Chapelle and Alexander Zien. Semi-supervised classification by low density separation. In *International Workshop on Artificial Intelligence and Statistics*, 2005.

Appendix

A More training details

We observed GPU executions to result in training time speed-ups of up to a factor of $O(10^2)$ compared to single CPU execution. For GPU training, we used NVIDIA Geforce GTX TITAN Black and NVIDIA Tesla K40 graphics cards.

Since the online learning rules have the structure of vector or matrix multiplications, they are ideally suited for parallelization on graphics cards. For parallel CPU computation, the concept of mini-batch training can be used: The learning effect of a small number ν of consecutive updates can be approximated by one parallelized update over ν independent updates. For GPU computation, we can use the same mini-batch training for optimization of GPU memory usage.

$$\Delta^\nu \omega_{cd}^{(n)} := \epsilon \sum_{i=0}^{\nu-1} \left(f_c(\vec{Y}^{(n+i)}, \omega^{(n)}) Y_d^{(n+i)} - f_c(\vec{Y}^{(n+i)}, \omega^{(n)}) \omega_{cd}^{(n)} \right) \quad (11)$$

$$\omega_{cd}^{(n+\nu)} \approx \omega_{cd}^{(n)} + \Delta^\nu \omega_{cd}^{(n)} \quad (12)$$

The maximal aberration caused by this approximation can be shown to be of $O((\epsilon\nu)^2)$. Since this effect is negligible for $\epsilon\nu \ll 1$, as shown in tab. A.1, we only consider the mini-batch-size ν as a parallelization parameter, and not as free parameter that could be chosen to optimize training in anything else than training speed and GPU memory load.

Table A.1: **Influence of mini-batch size on training results.** Averaged over 50 training runs for each setting, on a network with $C = 30$ hidden units using $N = 3000$ input patterns of the MNIST dataset and learning rates of $\epsilon_w = 0.5 \times C/N$ and $\epsilon_r = 0.5 \times K/N$, the mini-batch size shows no significant influence neither on the mean nor the variance of the test error or likelihood of the converged solutions.

mini-batch size	1	10	100
mean test error [%]	23.1 ± 0.2	23.2 ± 0.2	23.0 ± 0.2
std. dev. σ_{err} [pp]	1.27	1.26	1.24
mean log-likelihood	-836.472 ± 0.005	-836.468 ± 0.005	-836.475 ± 0.005
std. dev. σ_{ll}	0.034	0.032	0.036

A.1 Parameter tuning on 20 Newsgroups

Hidden units. For 20 Newsgroups it turned out, that already the complete setting, where $C = K = 20$, gives the best results on the validation set. Reasons for this can be the high dimensionality compared to the number of available training data points as well as the prominent noise when taking all words of a given document into account.

Normalization. To find a suitable normalization constant A , we perform experiments starting at $A = 70000 \gtrsim D$ for increasing values in steps of 1000 and evaluate the validation error. In the very low regime, the data patterns are for the system indistinguishable from background noise and the validation error is therefore very high. At the other extreme, with very high normalization constants, the softmax function will converge to a winner-take-all maximum function. A good value lies closely after the system is able to distinguish all patterns from background noise but when the normalization is still low enough to allow for a broad softmax response. For all our experiments on the 20 Newsgroups dataset we chose $A = 80000$.

Learning rates. We searched for the best parameter setting of the learning rates $\epsilon_{W/R}$ on a coarse scale over values of $\epsilon_w \in \{50, 20, 10, 5, 2, 1, 0.5\} \times C/N$ and $\epsilon_r \in \{5, 2, 1, 0.5, 0.2, 0.1, 0.05\} \times K/L$. We express the learning rate as proportional to C/N for the first hidden layer and proportional to K/L for the second layer, which represents the learning rate as proportionality factor to the average activation per hidden unit over one full iteration over a data set of N data points with L labels. Tuning this proportionality factor instead of the absolute value of the learning rate allows for scaling both in C and N , while keeping the same average learning speed per iteration. While every individual data point might have a weaker or stronger influence on learning, the average number of iterations over the full data set until convergence stays approximately constant. We found, that a relatively high learning rate in the first hidden layer yielded the best results on the validation set. Choosing such a large ‘step size’ can help to avoid early shallow local optima, but can also be harmful for overall precision. This trade-off is often encountered by using annealing schemes, that gradually decrease learning rates during training. However, for the sake of this paper we kept a constant learning rate throughout all training. For all experiments on this dataset, we chose $\epsilon_w = 5.0 \times C/N$ and $\epsilon_r = 0.5 \times K/L$ as free parameter setting.

A.2 Parameter tuning on MNIST

Hidden units. Contrary to the 20 Newsgroup dataset, for the MNIST dataset the validation error generally decreases with an increasing number of hidden units. We perform experiments over $C \in \{100, 200, 500, 1000, 2000, 5000, 10000, 20000\}$ and pick $C = 10000$ for all our experiments for both the recurrent and the feed-forward network. This represents a good trade-off between performance, required compute time, and possible overfitting effects due to the decreasing number of training data points per hidden unit.

Normalization. The dependence of the validation error on the normalization constant A shows similar behavior as for the 20 Newsgroups dataset. We increased A in steps of 25 starting at $A = 800 \gtrsim D$ and picked $A = 900$ as best value for all our experiments on MNIST.

Learning rates. While a high learning rate can be used to overcome early local optima, a lower learning rate will in general yield better results with the downside of a longer training time until convergence. This behavior we also observed on the validation set for MNIST. We performed experiments over settings of $\epsilon_w \in \{1, 0.5, 0.2, 0.1, 0.05, 0.02\} \times C/N$ and $\epsilon_r \in \{0.5, 0.2, 0.1, 0.05, 0.02\} \times K/L$ for a fixed maximum number of 200 iterations. As trade-off between performance and training time, we chose $\epsilon_w = 0.2 \times C/N$ and $\epsilon_r = 0.2 \times K/L$ for all experiments on MNIST.

B EM for normalized and hierarchical Poisson mixtures

To infer the model parameters $\Theta = (\mathcal{W}, \mathcal{R})$ of the deep mixture model eqs. (1) to (3) for given a set of N independent observed data points $\{\vec{y}^{(n)}\}_{n=1,\dots,N}$ with $\vec{y}^{(n)} \in \mathbb{R}_+^D$ and $\sum_d y_d^{(n)} = A \forall n$, we seek to maximize the data likelihood $\mathcal{L} = \prod_{n=1}^N p(\vec{y}^{(n)}|\Theta)$ using the Expectation Maximization (EM) algorithm. Instead of maximizing the likelihood directly, EM (in the form studied by [30]) maximizes a lower bound (the free energy) given by:

$$\mathcal{F}(\Theta^{\text{old}}, \Theta) = \sum_{n=1}^N \left\langle \log p(\vec{y}^{(n)}, c, k|\Theta) \right\rangle_n + H(\Theta^{\text{old}})$$

where $\langle \rangle_n$ denotes expectation under the posterior

$$\langle f(c, k) \rangle_n = \sum_c \sum_k p(c, k|\vec{y}^{(n)}, \Theta^{\text{old}}) f(c, k)$$

and $H(\Theta^{\text{old}})$ is an entropy term only depending on parameter values held fixed during the optimization of \mathcal{F} w.r.t. Θ .

The EM algorithm optimizes the free energy by iterating two steps: First, given the current parameters Θ^{old} , the relevant expectation values under the posterior are computed in the E-step. Given these posterior expectations, $\mathcal{F}(\Theta^{\text{old}}, \Theta)$ is maximized w.r.t. Θ in the M-step. Iteratively applying E- and M-steps locally maximizes the data likelihood.

C Approximate equivalence of neural online learning at convergence

In more detail, to derive eqs. (8), we first consider the dynamic behavior of the summed weights $\bar{W}_c = \sum_d W_{cd}$ and $\bar{R}_k = \sum_c R_{kc}$. By taking sums over d and c in eqs. (7), respectively, we obtain

$$\Delta \bar{W}_c = \epsilon_w s_c (A - \bar{W}_c), \quad \Delta \bar{R}_k = \epsilon_r t_k (B - \bar{R}_k). \quad (13)$$

As we assume $s_c, t_k \geq 0$, we find that for small learning rates the states $\bar{W}_c = A$ and $\bar{R}_k = B$ are stable (and the only) fixed points of the dynamics for \bar{W}_c and \bar{R}_k . This applies for all k and c and for any s_c and t_k that are non-negative and continuous w.r.t. their arguments.

The above result represents a generalization of the result obtained by [13] applied to two hidden layers instead of one. By assuming normalized weights based on eq. (13), we can approximate the effect of eqs. (7) as follows:

$$W_{cd}^{(n+1)} = A \frac{W_{cd}^{(n)} + \epsilon_w s_c(\vec{y}^{(n)}, \Theta^{(n)}) y_d^{(n)}}{\sum_{d'} (W_{cd'}^{(n)} + \epsilon_w s_c(\vec{y}^{(n)}, \Theta^{(n)}) y_{d'}^{(n)})} \quad (14)$$

and

$$R_{kc}^{(n+1)} = B \frac{R_{kc}^{(n)} + \epsilon_r t_k(\vec{s}^{(n)}, R^{(n)}) s_c(\vec{y}^{(n)}, \Theta^{(n)})}{\sum_{c'} (R_{kc'}^{(n)} + \epsilon_r t_k(\vec{s}^{(n)}, R^{(n)}) s_{c'}(\vec{y}^{(n)}, \Theta^{(n)}))} \quad (15)$$

where $W^{(n)}$ and $R^{(n)}$ denote the weights at the n th iteration of learning, where $\Theta^{(n)} = (W^{(n)}, R^{(n)})$, and where $\vec{s}^{(n)} = \vec{s}(\vec{y}^{(n)}, \Theta^{(n)})$ to abbreviate notation. Both equations can be further simplified. Using the abbreviations $F_{cd}^{(n)} = s_c(\vec{y}^{(n)}, \Theta^{(n)}) y_d^{(n)}$ and $G_{kc}^{(n)} = t_k(\vec{s}^{(n)}, R^{(n)}) s_c(\vec{y}^{(n)}, \Theta^{(n)})$, we first rewrite eqs. (14) and (15):

$$W_{cd}^{(n+1)} = A \frac{W_{cd}^{(n)} + \epsilon_W F_{cd}^{(n)}}{\sum_{d'} (W_{cd'}^{(n)} + \epsilon_W F_{cd'}^{(n)})}, \quad R_{kc}^{(n+1)} = B \frac{R_{kc}^{(n)} + \epsilon_R G_{kc}^{(n)}}{\sum_{c'} (R_{kc'}^{(n)} + \epsilon_R G_{kc'}^{(n)})}, \quad (16)$$

Let us suppose that learning has converged after about T iterations. If we now add another N iterations and repeatedly apply the learning steps, closed-form expressions for the weights $W_{cd}^{(T+N)}$ and $R_{kc}^{(T+N)}$ are given by:

$$W_{cd}^{(T+N)} = \frac{W_{cd}^{(T)} + \epsilon_W \sum_{n=1}^N F_{cd}^{(T+N-n)} \prod_{n'=n+1}^N (1 + \frac{\epsilon_W}{A} \sum_{d'} F_{cd'}^{(T+N-n')})}{\prod_{n'=1}^N (1 + \frac{\epsilon_W}{A} \sum_{d'} F_{cd'}^{(T+N-n')})} \quad (17)$$

and

$$R_{kc}^{(T+N)} = \frac{R_{kc}^{(T)} + \epsilon_R \sum_{n=1}^N G_{kc}^{(T+N-n)} \prod_{n'=n+1}^N (1 + \frac{\epsilon_R}{B} \sum_{c'} G_{kc'}^{(T+N-n')})}{\prod_{n'=1}^N (1 + \frac{\epsilon_R}{B} \sum_{c'} G_{kc'}^{(T+N-n')})}. \quad (18)$$

The large products in numerator and denominator of eqs. (17) and (18) can be regarded as polynomials of order N for ϵ_W and ϵ_R respectively. Even for small ϵ_W and ϵ_R it is difficult, however, to argue that higher-order terms of ϵ_W and ϵ_R can be neglected because of the combinatorial growth of prefactors given by the large products.

We therefore consider the approximations derived for the non-hierarchical model in [13], which were applied to an equation of the same structure as eqs. (17) and (18). At closer inspection of the terms $F_{cd}^{(T+N-n)}$ and $G_{kc}^{(T+N-n)}$, we find that we can apply these approximations also for the hierarchical case. For completeness, we reiterate the main intermediate steps of these approximations below:

Taking eq. (17) as example, we simplify its right-hand-side. The approximations are all assuming a small but finite learning rate ϵ_W and a large number of inputs N . Eq. (17) is then approximated by:

$$W_{cd}^{(T+N)} \approx \frac{W_{cd}^{(T)} + \epsilon_W \sum_{n=1}^N \exp\left(\frac{\epsilon_W}{A}(N-n) \sum_{d'} \hat{F}_{cd'}^{(n)}\right) F_{cd}^{(T+N-n)}}{\exp\left(\frac{\epsilon_W}{A} N \sum_{d'} \hat{F}_{cd'}^{(0)}\right)} \quad (19)$$

$$\approx \exp\left(-\frac{\epsilon_W}{A} N \sum_{d'} \hat{F}_{cd'}^{(0)}\right) W_{cd}^{(T)} + \epsilon_W \hat{F}_{cd}^{(0)} \sum_{n=1}^N \exp\left(-\frac{\epsilon_W}{A} n \sum_{d'} \hat{F}_{cd'}^{(0)}\right) \quad (20)$$

$$\approx \hat{F}_{cd}^{(0)} \frac{\epsilon_W \exp\left(-\frac{\epsilon_W}{A} \sum_{d'} \hat{F}_{cd'}^{(0)}\right)}{1 - \exp\left(-\frac{\epsilon_W}{A} \sum_{d'} \hat{F}_{cd'}^{(0)}\right)} = A \frac{\hat{F}_{cd}^{(0)}}{\sum_{d'} \hat{F}_{cd'}^{(0)}} = A \frac{\sum_{n=1}^N F_{cd}^{(T+N-n)}}{\sum_{d'} \sum_{n=1}^N F_{cd'}^{(T+N-n)}} \quad (21)$$

where $\hat{F}_{cd}^{(n)} = \frac{1}{N-n} \sum_{n'=n+1}^N F_{cd}^{(T+N-n')}$ (note that $\hat{F}_{cd}^{(0)}$ is the mean of $F_{cd}^{(n)}$ over N iterations starting at iteration T).

For the first step, eq. (19), we rewrote the products of eq. (17) and used a Taylor expansion (see supplement of [13] for details):

$$\prod_{n'=n+1}^N \left(1 + \frac{\epsilon_W}{A} \sum_{d'} F_{cd'}^{(T+N-n')}\right) \approx \exp\left(\frac{\epsilon_W}{A} (N-n) \sum_{d'} \hat{F}_{cd'}^{(n)}\right). \quad (22)$$

For the second step, eq. (20), we approximated the sum over n in eq. (19) by observing that the terms with large n are negligible, and by approximating sums of $F_{cd}^{(T+N-n)}$ over n by the mean $\hat{F}_{cd}^{(0)}$. For the last steps, eq. (21), we used the geometric series and approximated for large N (see supplement details of [13] for these last two approximations). Furthermore, we used the fact that for small ϵ_W , $\frac{\epsilon_W \exp(-\epsilon_W B)}{1 - \exp(-\epsilon_W B)} \approx B^{-1}$ (which can be seen, e.g., by applying l'Hôpital's rule).

By inserting the definition of $F_{cd}^{(n)}$ into eq. (21) we finally find:

$$W_{cd}^{(T+N)} \approx A \frac{\sum_{n=1}^N s_c(\vec{y}^{(n)}, \Theta^{(T+n)}) y_d^{(n)}}{\sum_{d'} \sum_{n=1}^N s_c(\vec{y}^{(n)}, \Theta^{(T+n)}) y_{d'}^{(n)}}. \quad (23)$$

Analogously, we find for R_{kc} :

$$R_{kc}^{(T+N)} \approx B \frac{\sum_{n=1}^N t_k(\vec{s}^{(n)}, R^{(T+n)}) s_c^{(n)}}{\sum_{c'} \sum_{n=1}^N t_k(\vec{s}^{(n)}, R^{(T+n)}) s_{c'}^{(n)}}, \quad (24)$$

where we again used $\vec{s}^{(n)} = \vec{s}(\vec{y}^{(n)}, \Theta^{(T+n)})$ for better readability in the last equation. If we now assume convergence, we can replace $W_{cd}^{(T+N)}$ by W_{cd} and $R_{kc}^{(T+N)}$ by R_{kc} , and we recover eqs. (8) in sec. 3 with converged weights W_{cd} and R_{kc} .

Note that each approximation is individually very accurate for small ϵ_W and large N . Eqs. (8) can thus be expected to be satisfied with high accuracy in this case and numerical experiments based on comparisons with EM batch-mode learning verified such high precision.

D More details on the compared algorithms including their testing protocols

In the comparison of sec. 4, SVM is a standard support vector machine and TSVM a version scalable to larger data sets and applicable in the semi-supervised setting [28]. Free parameters come in the form of kernel parameters, balancing constraint, parameters for preprocessing and auxiliary algorithms if applicable. In the case of the TSVM the free parameters are explicitly discussed in the paper. For small-scale experiments, [28] explicitly state for the TSVM that all its free parameters are tuned on the test set, and they refer to [31] to motivate such a protocol for algorithm comparison. For training on unlabeled data, the TSVM uses the *test set* and only in cases of more than 10 000 unlabeled data, the training set is added. This means that TSVM has seen the test set data points before classification. For parameter tuning TSVM uses a validation set (part of the training set) of 1000 data points.

AGR (or AnchorGraphReg) is an efficient graph construction algorithm used for data classification [25]. For MNIST, AGR seems to require relatively few free parameters for: graph regularization, sparsity, number of anchor points, number of nearest anchors, or dimensionality of PCA dimensionality reduction. Importantly, for the reported results in sec. 4, AGR uses training *and* test set for training. The authors write “We hold the [MNIST] training and test samples as a whole and randomly choose labeled samples from the whole set.” This implies that the algorithm has seen test data and probably at least some of its labels for training before it is evaluated (presumably on the standard test set).

MTC, AtlasRBF, Em^oNN, Em^{all}NN¹, and EmCNN are approaches that first aim to learn low-dimensional manifolds by using labeled and unlabeled data points before test data is classified. AtlasRBF [26] combines, for instance, a manifold learning approach [29] with a support vector classifier. It represents the algorithm with the best results for MNIST among a number of classifier/manifold learning combinations investigated. The free parameters of AtlasRBF consists for the manifold learning part of: manifold dimensionality, a weight sparsity penalty, and number of nearest neighbors that are taken into account. For the classification part, SVM kernel parameters are tuned. For the training and testing it is stated [26] that AtlasRBF uses the same protocol as AGR [25], i.e., the algorithm presumably sees test data points (and some of their labels) before testing.

MTC also learns low-dimensional manifold structure [22] combined with stochastic gradient descent for supervised learning of a neural network classifier. For the results reported in [22] a validation set is used for free parameter tuning. The size of the validation set is not given.

Em^oNN, Em^{all}NN¹, and EmCNN as well as all data on MNIST in [27] use the same training and testing protocol as used for the TSVM in [28]. This means that: unlabeled test data has been seen and used by the algorithms before the test performance is measured; and that free parameters were presumably tuned on the validation set of 1000 data points.

The M2 model of [24] combines a generative model approach with a deep neural network to connect hidden to observed variables. Free parameters include learning rate, first order decay and second order decay parameters for weights. We found no statement on the hyper-/free-parameters of the used deep neural network architecture in the paper, and no mentioning of a validation set. The source code published together with the paper [24] does contain a validation set of 10 000 data points, however. We therefore assumed such a validation set for comparison in sec. 4.

The model M1 also reported in [24] is a latent variable model for feature learning combined with a deep network and a classifier such as TSVM but we found it difficult to deduce details on free parameters and tuning protocols. The models M1 and M2 can themselves be combined representing a large heterogeneous system with many free parameters.

The DBN-rNCA approach combines Neighbourhood Component Analysis (NCA) with deep Restricted Boltzmann Machines [23]. A typical setup consists of four layers (three hidden) for encoding and four layers (three hidden) for decoding and a middle layer, with an architecture for MNIST being (500, 500, 2000, 30, 2000, 500, 500) for the number of hidden units from bottom to top respectively. For the reported results, a set of 10 000 data points taken from the training set was used as validation set.

The discriminative RBM [20] that we used for comparison of the 20 Newsgroups data also provides a result on MNIST. For 800 labeled training points and a validation set of 200 labeled data points, the semi-supervised “semi-sup HDRBM” results in a test error of 8.04%. This is in the range of the standard SVM of sec. 4 but note that just 5000 unlabeled data points were used for training (we therefore did not include this test error in sec. 4).

In summary, the protocols to train, tune and test the algorithms compared to in sec. 4 are unfortunately very diverse. Data is deduced from the papers where the classification errors used for sec. 4 are reported. Also sometimes protocols

had to be inferred from context. In general, the deduced data was done to the best of our knowledge but we found it to be a very difficult task. The list is not exhaustive but we believe that we included the currently best performing algorithms according to the reported test error.